Available online at www.sciencedirect.com
SCIENCE DIRECT®
Journal of Catalysis 220 (2003) 317–325
JOURNAL OF CATALYSIS
www.elsevier.com/locate/jcat

Active sulfated alumina catalysts obtained by hydrothermal treatment

M.L. Guzmán-Castillo, E. López-Salinas, J.J. Fripiat, J. Sánchez-Valente, F. Hernández-Beltrán,* A. Rodríguez-Hernández, and J. Navarrete-Bolaños

Instituto Mexicano del Petróleo, Eje Central L. Cárdenas 152, AP 14-805, 07730 México DF, Mexico

Received 4 March 2003; revised 20 May 2003; accepted 28 May 2003

Abstract

The structural and surface properties of sulfated γ-Al_2O_3 prepared by hydrothermally aging precipitates obtained from aluminum sulfate and ammonia have been studied. The Lewis sites are formed on coordinately unsaturated fourfold alumina. No pentacoordinated aluminum has been found, probably as a consequence of the aging process. Residual sulfate is distributed among several species characterized by their desorption temperatures. Brönsted sites of high strength are probably located on sulfate species desorbing between 900 and 1000 °C. They may have the following schematic structure $(O=)_2S(–OH)(–O–Al)$. The decomposition of 4-methylpentan-2-ol shows clear differences according to the types of acidity present on the surface. The sulfated aluminas have favorable textural properties: pore size $\cong$50 nm and specific surface area $\cong$200 m^2/g stable up to more than 700 °C.

Keywords: Sulfated alumina; Hydrothermal preparation; Acid sites; Catalytic properties

1. Introduction

γ-Al_2O_3 is widely used as catalysts or catalyst supports, because of its thermally stable surface area bearing Lewis acid sites, its textural stability, keeping open pores with diameters of the order of 5 nm up to above 700 °C, and its low cost. Reinforcing the acid strength of the surface by impregnation with sulfuric acid, and thus grafting Brönsted sites, has inspired many studies. Tanabe [1] has reviewed the subject at the beginning of the seventies while 20 years later, Arata [2] studied in detail the properties of solid superacids made of sulfated supported metal oxides.

The pioneering studies of Tanabe et al. [3] and Corma [4], attracted much attention from numerous research groups to follow up their findings and focus on the most promising sulfated metal oxides, that is, mainly on sulfated ZrO_2, because of its stronger acidity than most other sulfated metal oxides. Evidently, other sulfated metal oxides were neglected or not studied in more detail, in comparison with sulfated zirconia. Sulfated aluminum oxy-hydroxides or oxides were not considered as attractive as their more active ZrO_2, TiO_2, and SnO_2 sulfated counterparts, with acid strengths ca. 100 times higher. For instance, in terms of reaction rate, sulfated ZrO_2, TiO_2, and Fe_2O_3 in the gas-phase isomerization of cyclopropane at 100 °C were 3.5, 3.3, and 2.9 times more active than sulfated alumina [5].

On the other hand, the nature and structure of different surface acid sites on a given metal oxide have tremendous impact on the selectivity for a particular reaction. For instance, H_2SO_4, or H_3PO_4 supported on SiO_2, Al_2O_3, and SiO_2–Al_2O_3 exhibit high activities and selectivities for various organic syntheses [6]. Hence, the development of a solid acid having different acid site types and amounts is an important challenge for several industrial processes [6].

From the viewpoint of plausible catalyst applications, it is highly desirable to form strong acid sites on aluminum oxy-hydroxides, instead of on other metal oxides, because there is already a huge infrastructure for producing alumina in various physical forms. A few studies pursuing the formation of strong acid sites on aluminum oxy-hydroxides have partially advanced this task.

Highly acidic γ-Al_2O_3 was prepared [2] by exposing γ-Al_2O_3 to 2.5 M H_2SO_4 followed by calcining in air at about 600 °C. An acid strength of $H_0 \cong -14.5$ (indicator technique) was found after calcination at 650 °C.

Yang et al. [7] have reported that various sulfate species are created by treating γ-Al_2O_3 by H_2SO_4 aqueous solutions of various concentrations. DTG peaks at 630, 800,

* Corresponding author.
E-mail address: fjhernan@imp.mx (F. Hernández-Beltrán).

0021-9517/$ – see front matter
doi:10.1016/S0021-9517(03)00266-5

and 950 °C were assigned to "a surface sulfate, a multilayer surface sulfate and a crystalline aluminum sulfate," respectively. The surface sulfate is the main species for H_2SO_4 concentrations smaller than 0.8 M. It could induce Lewis super acidic sites able to isomerize *n*-butane at 300 °C.

Ferreira and Rueda [8] have focused their attention on the prevalent role of Brönsted sites in the structural and double-bond isomerization of *n*-butene on sulfated alumina. Two surface models were presented: reaction of SO_3 with two adjacent surface OH to generate a dioxo species SO_2 or reaction of SO_3 with a Lewis acid site generating a monoxo species 3(O–S)=O, easily convertible into a Brönsted site.

The importance of surface loading on the acid properties is unanimously recognized, but the direct formation of sulfated γ-Al_2O_3 by hydrolysis of $Al_2(SO_4)_3$ has not attracted the attention that it deserves [9].

Guzmán-Castillo et al. [10] have autoclaved precipitates for 18 h, obtained by treating aluminum sulfate with ammonium hydroxide between 50 and 240 °C. In this study, the effect of the temperature of hydrothermal aging on precipitated aluminas (from aluminum sulfate) was examined, with the aim of finding crystal size and acidity correlations. With the aid of FT-IR of adsorbed pyridine, the nature of acid sites was revealed. Finally, well-characterized sulfated aluminas were selected and tested as catalysts in the 4-methylpentan-2-ol decomposition, as a model reaction. The presence of strong Brönsted acid sites was evidenced by skeletal isomerization.

2. Experimental

2.1. Preparation

A gel was obtained from $Al_2(SO_4)_3 \cdot 18H_2O$ (Aldrich, 98%) and NH_4OH (28%), added in stoichiometric amounts at room temperature, the pH being between 7 and 8. The precipitate was transferred into a 2 L autoclave where it was treated for 18 h between 25 to 240 °C which defined what we called the aging temperature (hereinafter the aluminas will be referred to as B-X, where X corresponds to the hydrotreatment temperature). The gel was then filtered, washed with bidistilled water, and dried at 100 °C. The resulting solid was calcined at 600 °C for 4 h.

2.2. Techniques

Most of the techniques used to study our solids are classical or have been described elsewhere [11]. They will be noted briefly.

2.2.1. X-ray powder diffraction

Dried and calcined samples were studied in a Bruker Advance D-8 equipment. The X-ray powder diffraction patterns of the samples packed in a glass holder were recorded at room temperature with Cu-K_α radiation, θ–θ, diffractometer, equipped with a graphite secondary-beam monochromator. Diffraction intensity was measured between 10 and 110°, with a 2θ step of 0.02° for 8 s per point.

2.2.2. Textural analysis

Specific surface area and pore-size distributions were obtained from nitrogen adsorption–desorption isotherms measured in an automatic Micromeritics ASAP-2100 analyzer. The adsorption was carried out on annealed solids, after outgassing at 400 °C, respectively, for 4 h under a residual pressure of 10^{-5} Torr.

2.2.3. Acidity

FTIR-pyridine adsorption technique was used to determine the types of acid sites on calcined samples. Experiments were carried out in a Fourier transform infrared (FTIR) spectrometer Perkin-Elmer Model 170-SX. Prior to pyridine adsorption, the samples were outgassed and then heated to 500 °C at 20 °C/min and cooled to room temperature. After this pretreatment, they were exposed for 20 min to saturated pyridine vapor. After adsorption, infrared spectra were recorded after outgassing at 50, 100, 200, 300, and 400 °C.

2.2.4. Sulfur content

The sulfur content was determined at 1350 °C in a LECO analyzer, Model SC-444, fitted with an infrared detector.

2.2.5. IR spectroscopy

FTIR spectra were recorded on a Nicolet Protege 460, with a resolution of 4 cm^{-1}. The powder was pressed into KBr (2%) thin disks and analyzed in a Pyrex cell fitted with CsI windows.

2.2.6. Differential gravimetric analysis

Weight loss and temperatures associated with phase transformations were determined by thermogravimetry and differential thermal analysis with a Perkin-Elmer TG-7 and a Perkin-Elmer 1700 apparatus, respectively. Samples were heated in a static atmosphere from room temperature to 1400 °C at 10 °C/min.

2.2.7. ^{27}Al MAS NMR

One-pulse spectra were recorded at 130.3 MHz, when spinning at 11.5 kHz, with a tip angle of less than B/12 in order to reduce the content in nonvisible Al. The pulse duration was 1 s and the recycling time was 1 s, and 256 scans were accumulated.

2.2.8. Catalytic test

The calcined solids were studied as catalysts in the gas-phase decomposition of 4-methylpentan-2-ol (4Me2Pol). The reaction was carried out in a fix-bed quartz tubular reactor fed by He (as carrier gas) containing a given amount of 4Me2Pol. All stainless-steel tubing in and out of the

reactor was heated at 100 °C in order to avoid condensation of the reactant and products. The reaction conditions were 100–130 °C, WHSV $= 8.32 \times 10^{-3}$ h^{-1} (or $W/F = 0.0807\ g_{cat}\ h\ g_{react}^{-1}$), atmospheric pressure, 50 mg of catalyst. Operating conditions were set in order to keep conversion under 10% in order to guarantee differential conditions. Prior to reaction, the solids were flushed with anhydrous He at 500 °C for 1 h and then brought to reaction temperature. The reaction products were analyzed on-line every 20 min by means of an automatic six-port sampling valve connected to a Varian Star 3600 CX gas chromatograph equipped with a flame ionization detector. A 50-m capillary PONA column was used to separate the products. All products were identified and quantified by comparison to the analysis performed with commercial pure compounds.

3. Results

3.1. XRD and TGA-DTA results

The analytical results are shown in Table 1. XRD patterns showed poor crystallization of dried samples B-25, B-50, and B-100. The solids are mixtures of pseudo-boehmite, some crystallized $Al_2(SO_4)_3$, and some amorphous constituents. By contrast, samples synthesized above 100 °C clearly showed the boehmite phase with different crystallinity.

With pure boehmites DTA studies have shown a wider endothermic peak below 200 °C due to the removal of hydration water and an endothermic peak at higher temperatures related to phase transition to γ-Al_2O_3 [11,15]. Variations between 380 and 528 °C of the transition temperature were observed depending on the boehmite crystal size [15]. In the present case the presence of amorphous phases in samples B-25, B-50, and B-100 produced a number of relatively well-defined DTA endothermic peaks while with samples obtained above 100 °C thermograms attributable to well-defined boehmite were observed. This difference is illustrated in Fig. 1 for samples B-50 and B-140. With samples B-25 and B-50, up to three endothermic peaks were observed below 500 °C and up to three above that temperature. Four endothermic peaks were observed with B-100 below 500 °C and one more near 750 °C. The characteristic peaks were observed at 630, 800, and 950 °C as reported by Tsien-syh Yang et al. [7] for γ-Al_2O_3 treated with H_2SO_4. As the aging temperature increased, the 630 and 800 °C peaks weakened while the high-temperature peak subsisted and broadened.

Table 1
Precipitation from aluminum sulfate by ammonia: effect of aging temperature

Sample	BET[a] (m^2/g)	H_2O/Al_2O_3[b]	Boehmite cont. (a.u.)	Sulfur load[a] (%)	Crystalline phase(s)	510 °C peak width (a.u.)
B-25	71	3.31	4	6.48	Multi	
B-50	88	3.51	11	5.86	Multi	0.5
B-100	126	3.35	11	4.70	Multi	0.25
B-140	248	1.4	19	2.38	Boehmite	0.24
B-180	136	1.13	24	< 1	Boehmite	0.082
B-240	56	≅ 1		< 1	Boehmite	

[a] Samples calcined at 600 °C for 4 h.
[b] From TGA.

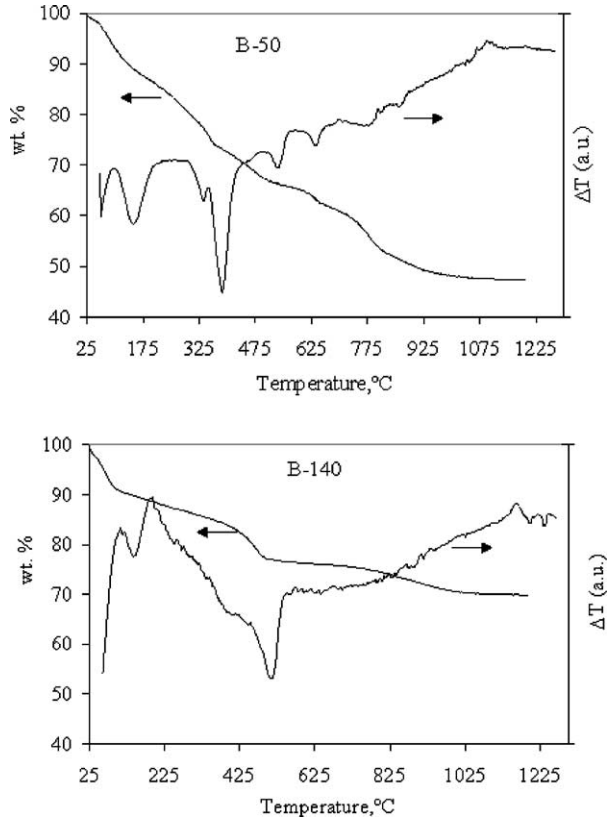

Fig. 1. Differential thermal and gravimetric analyses of B-50 and B-140.

The ease of the sulfate elimination from the gel depends on the temperature of the hydrothermal treatment. It is a general observation that the extent of the crystallization into boehmite depended on the removal of the counteranions and hence favoring the diffusion of anions out from the gel by thermal activation is a prerequisite for crystallization to take place [12]. In this case, we plotted the logarithm of both the boehmite content (arbitrary units, a.u.) and the width of the endothermic peak where boehmite to γ-Al_2O_3 transition takes place, as a function of the inverse of the absolute temperature of aging (see Fig. 2). Phase transition was verified by XRD and the boehmite content was obtained from the DTA's endothermic peak and the relative amount of weight loss assuming the stoichiometry $AlOOH \rightarrow H_2O + Al_2O_3$. The temperature coefficient calculated from the slope of the line was ca. 6 kcal/mol, an acceptable value for diffusion.

The width of the endothermic peak observed at ≅ 510 °C sharpened as the boehmite crystallinity increased, in agreement with an observed increase of crystallite dimensions [11]. Thus, aging temperatures above 100 °C favored the removal of the sulfate species. The residual sulfur content in calcined samples shown in Table 1 is consistent with this.

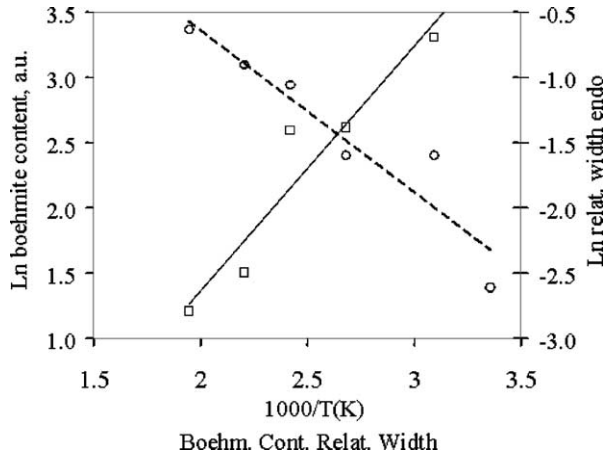

Fig. 2. Logarithmic variation of boehmite content and of its crystallinity (width of the endothermic peak at 510 °C) as a function of inverse of aging temperature (○, boehmite content; □, relative width).

3.2. The aluminum coordination

As boehmite looses its constitutional OHs, a transition γ-Al_2O_3 is formed. The poorly organized nanosized transition alumina is characterized by a distribution of aluminum within three coordination states, observable by high-resolution solid-state NMR. Besides the fourfold and sixfold coordinated aluminum, typical for a spinel, Al^V, pentacoordinated aluminum is eventually observed.

According to Chen et al. [13], Al^V is an unstable state of coordination. For instance, in a ground boehmite, calcined at 600 °C for 1 h, the Al^V NMR signal is as strong as the Al^{IV} signal, but it decreases to half its intensity after calcination at 700 °C for 1 h and disappears after calcination at 800 °C. In another transition alumina, calcination at 600 °C for 1 h suppresses the pentacoordinated Al.

Al^V was not observed in the calcined sulfated γ-Al_2O_3 described in Table 1. The ^{27}Al MAS NMR spectra, as shown in Fig. 3 for samples B-180 and B-100, are all alike and typical of alumina spinels containing about 1/3 of Al^{IV}.

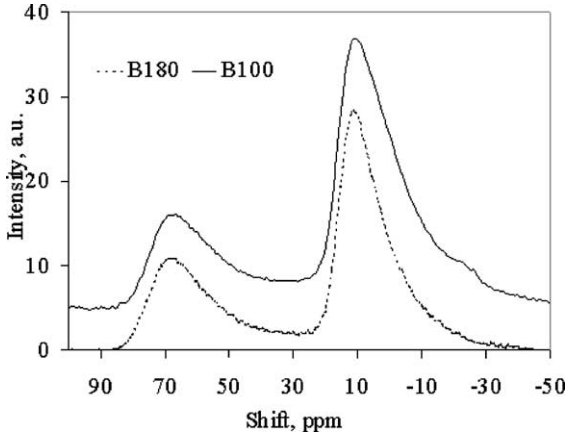

Fig. 3. ^{27}Al NMR of sulfated and hydrothermally aged B-100 and B-180 γ-Al_2O_3s.

Findings by Coster and Fripiat [14] help to explain the absence of Al^V. The hydrothermal aging increases the polymerization of the structural units, containing sixfold coordinated aluminum, Al^{VI}, and the number of structural defects to which Al^V is associated decreases accordingly. The *020* reflection used by Bokhimi and co-workers [11,15] to calculate the dimension d, or thickness, perpendicular to the *020* plane of boehmite, could measure the degree of polymerization. However, when aged under hydrothermal conditions, d_{020} of the precursor is beyond the limit for observing Al^V in the resulting alumina after dehydroxylation. Thus in the alumina samples studied here, the only Lewis site is Al^{IV}.

3.3. Acidity and identification of the sulfate species

The IR spectra of chemisorbed pyridine after outgassing at increasing temperature are presented in Fig. 4. In Table 2, the corresponding weight loss at 950 °C obtained from TGA was assigned to the removal of SO_3 (expressed in μmol/m^2), in order to allow comparison with the number of Brönsted sites, obtained by pyridine titration using IR spectroscopy. The amount of adsorbed pyridine (coordinated or pyridinium ion) was estimated using methods reported elsewhere [16,17]. It is worth noting that the acid density (pyridine titration at 50 °C) in γ-Al_2O_3 samples obtained by sol–gel and hydrothermal aging ranged between 1.1 and ca.

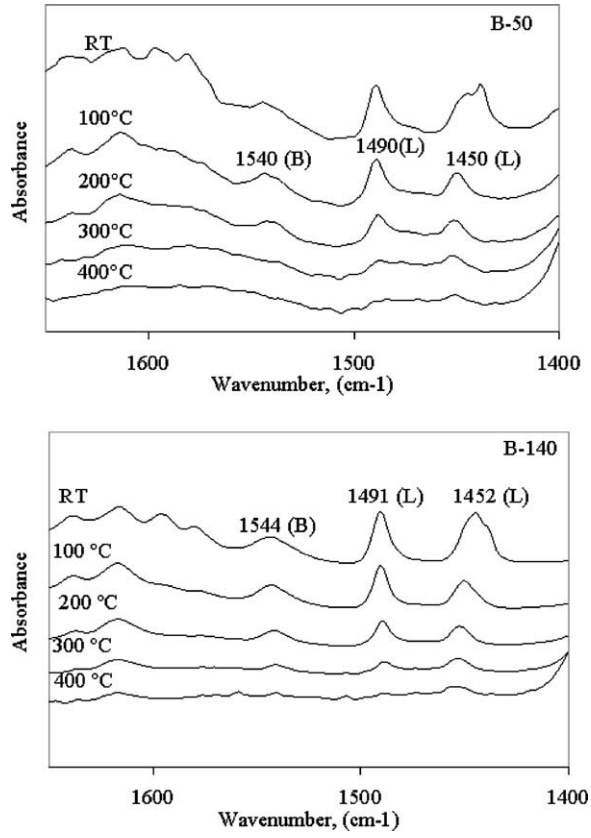

Fig. 4. Desorption of pyridine and pyridinium at increasing temperatures from B-50 and B-140.

Table 2
Surface density of Brönsted (BAS) and Lewis (LAS) acid sites (μmol/m^2), from the IR spectra of pyridine adsorbed at 50 °C, weight loss at 950 °C (wt%), and Brönsted sites contribution related to the high-temperature sulfate (HTS) content

Sample	BAS[a]	LAS[a]	Weight loss at 950 °C	Contribution of BAS (%) to HTS
B-50	0.59	2.28	4.4	13.4
B-100	0.97	1.64	2.2	44.0
B-140	0.6	1.39	1.2	48.9
B-180	0	4.15	≅ 0.4	0
B-240	0	4.02		0

[a] Temperature corresponding to these retentions has been chosen arbitrarily at 50 °C.

2.0 μmol/m^2 [18], lower than the values obtained with sulfated aluminas in the present case.

There is no direct evidence that the weight loss at 950 °C is only due to the removal of SO_3. The removal of hydration and of constitution water occurs for the most part below 600 °C, although spinels may contain some residual protons. However, considering this high temperature, the assumption made by neglecting these extra protons is acceptable.

The classical assignments of the Brönsted and Lewis sites are 1543 and 1452 cm^{-1}, respectively. The corresponding contents per unit area are shown in Table 2. The Brönsted sites content obtained directly from the analysis of the IR spectra represents about 50% of the high-temperature sulfate (HTS), but HTS is less than 41% of the total S loading, shown in Table 1.

Infrared spectra of KBr pellets were run in order to obtain information on the molecular structure of the sulfate groups; see Fig. 5. As the amount of adsorbed water is reduced by heating between room temperature and 300 °C, the broad band at ca. 3500 cm^{-1} shifted toward higher frequency because of the decreasing contribution of the hydrogen-bonded water to OH groups. The intensity of the shifted hydroxyl stretching near 3550 cm^{-1} was plotted against the water content measured by the absorbance at 1630 cm^{-1}. The intercept represents the remaining surface OH after the elimination of water. The residual OH content is represented qualitatively in absorbance units in Table 3.

The temperature for which the elimination of adsorbed OH is completed is between 300 and 400 °C. Above this temperature the OH content is almost constant until a higher temperature. This behavior is common to most oxides and there is no experimental evidence that these residual OHs play a role in Brönsted acidity of sulfated alumina.

According to Yamaguchi et al. [5], the photoelectron spectroscopy of S ($2P_{3/2}$) reveals that the sulfur in the active site is in the 6+ oxidation state while the IR spectroscopy shows a characteristic strong band at 1398 and 1390 cm^{-1} in sulfated alumina and sulfated zirconia, respectively. This band is accompanied by broad bands between 1200 and 900 cm^{-1}. Similar IR observations are reported by Waqif et al. [19] and by Bensitel et al. [20]. In sulfated zirconia, calcined at 550 °C, Sohn and Kim [21] have assigned bands at 1207, 1136, and 1053 cm^{-1} to ν_3 vibrations of bidentate SO_4^{2-} in a C_{2v} symmetry. Molecules of the XY4 type have nine normal modes of vibration whose infrared or Raman activities depend on molecular symmetry. In the usual Td (tetrahedral) symmetry, the ν_3 and ν_4 are IR active and triply degenerated. In the C_{2v} symmetry the degeneracy is lifted up and the three ν_3 and ν_4 bands are IR active [22]. This is probably what happens here.

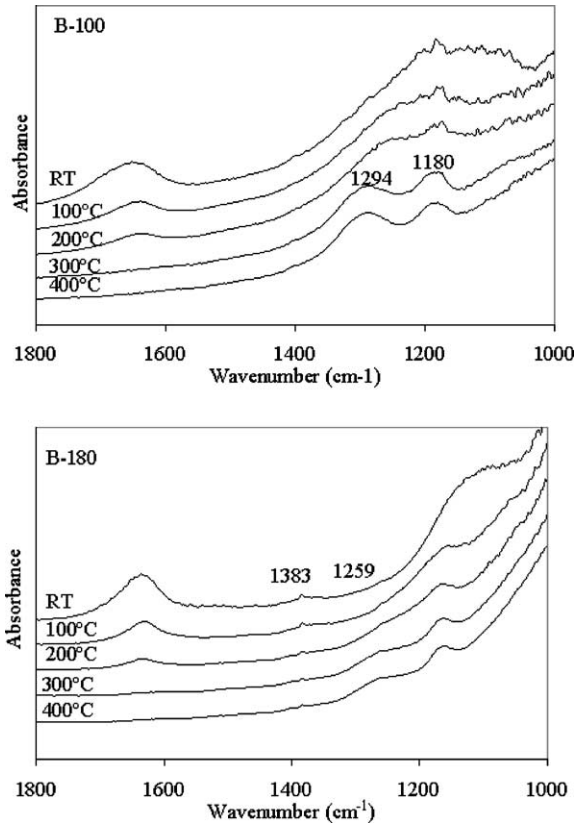

Fig. 5. Example of IR spectra of B-100 and B-180 in KBr pellets after calcination at 600 °C, rehydration in air, and outgassing at RT, 100, 200, 300, and 400 °C, top to bottom.

Table 3
IR bands, not due to H_2O, observable between 4000 and 1000 cm^{-1} and aproximate intensity (absorbance units)

Sample	OH	S=O asym. stretching	S–(OH) stretching	S=O sym.	S–(OH)[b]
B-100	3530[a] (0.45)	1409	1293[a] (0.28)		1180[a] (0.15)
B-140		1388	1296[a] (0.08)	1250 (0.07)	1181[a] (0.04)
B-180	3545[a] (0.6)	1383	1295[a] (0.03)	1259 (0.04)	1153[a] (0.09)
B-240	3575[a] (0.3)	1383		1257	

[a] Sensitive to the presence of adsorbed water.
[b] Not assigned.

The semiquantitative results obtained for the sulfated alumina are described in Table 3. A first remark (see Fig. 5) can be made about the weakness (but sharpness) of a band located near 1400 cm^{-1} and observed in all samples. This band is not as strongly sensitive to the presence of adsorbed water as it should be if it were a surface S=O stretching.

A high sensitivity was observed in sulfated zirconia [23], where the band near 1400 cm^{-1} becomes a strong band after calcination at 550 °C and partial rehydration. There [23,24] it was assigned to S=O stretching of SO_3. Nothing similar was observed in this work with sulfated aluminas. Instead bands at 1295 cm^{-1}, and to a lesser degree, at 1181 cm^{-1} are observable only upon water removal. There are especially well developed in B-140 and B-100, the samples with the highest content in Brönsted sites, but are not observable in B-180. It is therefore tempting to assign them to an S–(OH) stretching vibration.

From a detailed study of the dehydration–rehydration process of sulfated zirconia, Babou et al. [23] consider the reversible effects of water on the adsorbed surface species and suggest the following assignments:

(a) Bidentate: SO_4^{2-}, ν_3, 1207, 1136, and 1053 cm^{-1}; ν_1, 997 cm^{-1}.
(b) HSO_4^-: 1322 and shoulder at 1200 cm^{-1}.
(c) H_2SO_4: 1368, 1250, 1040, and 853 cm^{-1}.
(d) SO_3: 1387–1393, 1027, and 953 cm^{-1}.

Therefore, we suggest the bands at 1294 and 1180 cm^{-1} be assigned to HSO_4^-. They are shifted by about 20 cm^{-1} being bonded to the alumina network, and possibly to a CUS site.

The exact nature of the bonds of HSO_4^- with the lattice cannot be established with certainty. A species such as depicted in the discussion could reconcile the various observations and respect the 6+ charge of sulfur.

3.4. Catalytic 4-methylpentan-2-ol decomposition

Decomposition of 4Me2Pol (Fig. 6) is catalyzed by solid acids to yield dehydration-skeletal isomerization products and/or solid bases to dehydrogenate the alcohol to the parent ketone [25,26]. Depending on the acid site strength, various products can be formed. Thus, *A* product will form on weak acid sites and *B* products (*cis* and *trans*) will require intermediate acid strength. *C* Products, from double-bond shift reactions, will require stronger acid sites, while *D* products from skeletal isomerization will need very strong acid sites.

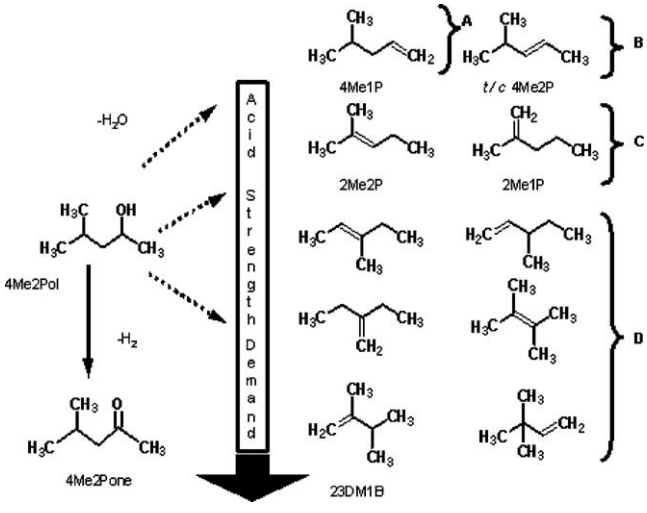

Fig. 6. Reactions involved in the decomposition of 4Me2Pol. Note the different dehydration (dashed arrows) and dehydrogenation (solid arrow) paths. Products were grouped according to their increasing acid strength demand: $A < B < C < D$.

In order to examine the acid strength of our sulfated aluminas, two samples were used as catalysts for the decomposition of 4Me2Pol: B-50 which contained both Brönsted and Lewis sites, and B-180 which had exclusively Lewis acidity (see Table 2). B-180 contained twice as many Lewis sites as B-50.

The conversion evolution for these two aluminas indicated that B-50 was more active than B-180 as shown in Fig. 7. In fact, for B-50 a lower reaction temperature was required in order to keep conversion under differential conditions. It appears that the higher initial conversion may be due to Lewis acid surface sites, which can become deactivated by formation of Al–OH groups from water (a by-product of the alcohol dehydration) during the initial stages of reaction. Following this deactivation, Brönsted acid sites become important in maintaining the catalytic activity.

Moreover, the selectivity (Fig. 8), corresponding to different acid strength demands, differed for these two aluminas. B-180, which lacks Brönsted sites, yields products associated to weak (*A*), intermediate (*B*), and strong (*C*) acid sites, that is, dehydration and double-bond shift products. Clearly, the Lewis sites were strong enough to catalyze the double-bond shift. In contrast B-50, which was made up of both Brönsted and Lewis sites, yields *A*, *B*, *C*, and *D* products. The later is associated with very strong acid sites necessary for skeletal isomerization. These observations suggest that Brönsted sites are responsible for reaction *D*. Noteworthy, double-bond shift products (*reaction C*) were lower when using B-50, thus suggesting that its Lewis acid sites are not as strong as those in B-180.

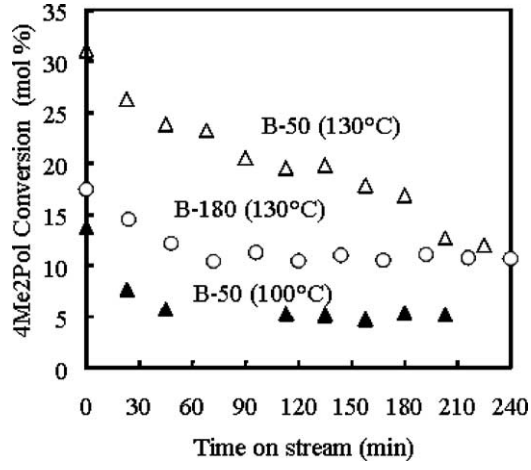

Fig. 7. Evolution of 4Me2Pol conversion on B-50 and B-180 at 100 and 130 °C.

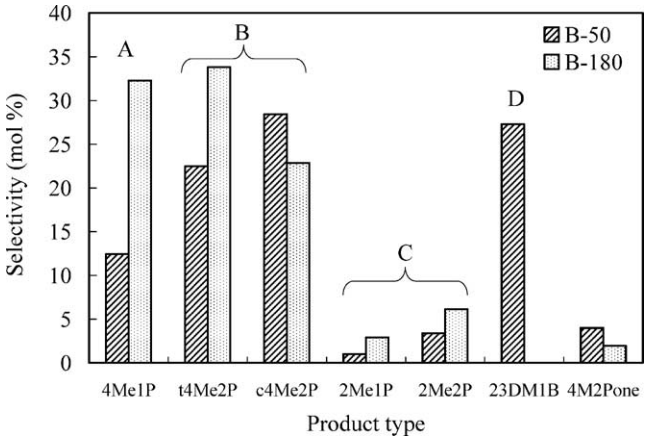

Fig. 8. Selectivity to 4Me2Pol decomposition products using B-180 and B-50 at 130 °C. Products were grouped according to their increasing acid strength demand: $A < B < C < D$.

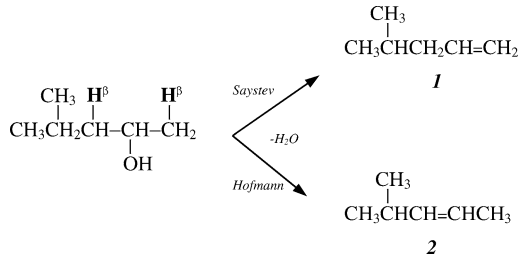

Scheme 1. Saystev and Hofmann dehydration routes.

In substrates where alternative β-hydrogen atoms are available, as in 4Me2Pol, it is possible to obtain more than one alkene on elimination (see Scheme 1). In our case, 4-methylpent-2-ene *1* will come from a Saystev orientation and 4-methylpent-1-ene *2* will derive from a Hofmann orientation [27]. The 4-methylpent-2-ene/4-methylpent-1-ene (2-ene/1-ene) ratio is 4.0 in B-50 and 1.8 in B-180. Clearly the base and acid sites on these two aluminas affect in a different way the conformation of the 4Me2Pol transition state (TS) favoring one of those orientations.

Sample B-50, with both Brönsted and Lewis features, had a marked tendency toward Saystev orientation (e.g., 2-ene). This could be explained considering that the C–OH bond in 4Me2Pol is relatively readily broken. As the attacking base begins to break the H–C^{β} bond, the C–OH bond becomes fragile. Thus the double bond will be formed earlier in the overall process, i.e., the transition state will have a great deal of double-bond character, and it will be stabilized by alkyl groups fixed on the double bond. In other words, the attacking base will tend to remove preferentially β-H, leading to the more stable alkene.

In the alumina made up exclusively of Lewis sites, B-180, Hofmann orientation (1-ene) becomes important in comparison with that in B-50. This indicates that the C–OH bond in 4Me2Pol is relatively less easily broken, and that the removal of a β-H by the attacking base will proceed further before the C–OH bond begins to break. The TS will be less "alkene-like" and more "carbanion-like" in character;

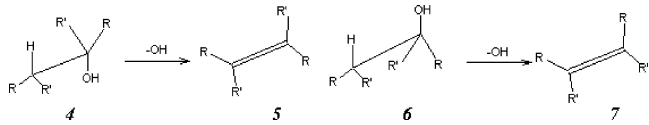

Scheme 2. *Cis* 2-ene and *trans* 2-ene orientations from alcohol dehydrations.

it will thus be stabilized by a lack of alkyl substitution at the carbanion carbon atom (i.e., the relative stability of carbanions is primary > secondary > tertiary). In order to proceed simultaneously, acidic and basic sites operating on this 1, 2 elimination may have strengths similar to those of C–OH and β-H bonds, respectively.

The attacking base will tend to remove preferentially that β-H which leads to more stable carbanion-like TS, or to a 1-ene product. Base and acid sites in this alumina have differing strengths than those required to break β-H and C–OH bonds, respectively. Base sites have strengths closer to β-H bonds than acid sites to C–OH bonds.

Trans to *cis* (*t/c*) 4-methylpent-2-ene stereoselectivity can be used to shed light on the degree of interaction of medium acid sites with the TS of 4Me2Pol (Scheme 2). The less energy demanding conformation, antiperiplanar **4**, leading to *trans* 2-ene **5** isomer is the preferred one over the *syn*-periplanar **6** which yields the *cis* 2-ene **7** isomer.

B-180 (Lewis sites only) showed a *t/c* ratio of 1.8, while in B-50 (Brönsted and Lewis acid sites) it was 0.8. Thus, acid sites in B-50 had a higher degree of polarization since the less energetically favored **7** was formed (Scheme 2).

4. General discussion

The magnitude ($\cong$50%) of the contribution of Brönsted sites, obtained from the IR spectrum, to the HTS weight loss, supports the hypothesis that this species is linked to protonic acidity.

On the basis of the IR results, we suggest the following surface structure in which an S=O bond is shared with a CUS site and an S–O– bond with a surface Al. This scheme emphasizes the role of neighboring Lewis sites, the strength of the Brönsted sites being related to the electron-accepting power of the neighboring Al^{IV} Lewis site. The higher electronegativity of ZrO_2, (0.78), compared to Al_2O_3, (0.60), could justify why, on alumina, (Scheme 3), it should be preferred. On ZrO_2, chemisorbed SO_3 species would better explain the strong Lewis properties [23,24].

With such an anchoring to the framework, the active species could stand high temperature and, by hydrolysis of the S–O–Al bond and its replacement by one OH, H_2SO_4

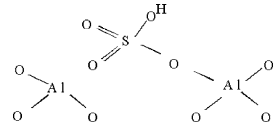

Scheme 3. Surface structure of sulfated γ-Al_2O_3.

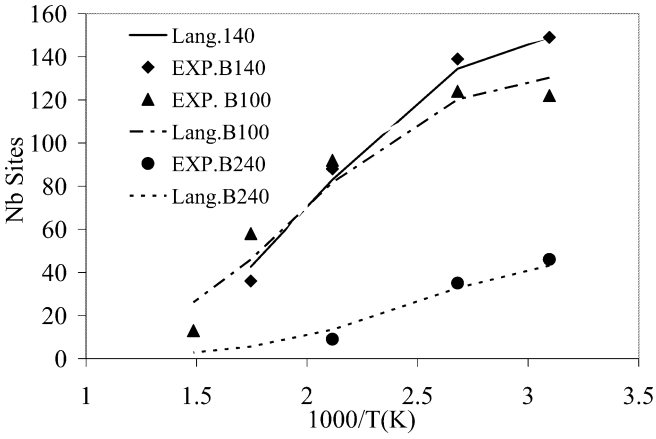

Fig. 9. Variation of the number of pyridinium cations (Brönsted sites) with respect to the inverse of temperature, $1000/T$ (K). Lines represent Eq. (1).

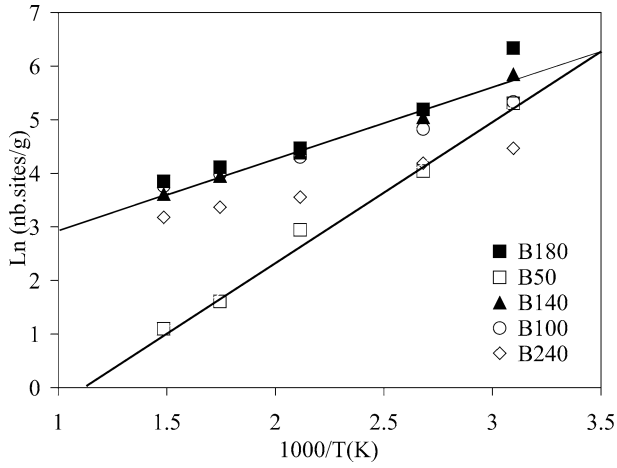

Fig. 10. Variation of the number of pyridine molecules chemisorbed on Lewis sites with respect to the inverse of temperature, $1000/T$ (K). Lines represent Eq. (2).

could be formed easily upon rehydration. This transformation would be reversible, as observed on sulfated zirconia.

Gruver and Fripiat [29] have approximated the strengths of Lewis and of Brönsted sites from the temperature-activated desorption energy of chemisorbed ammonia. A calorimetric study of ammonia adsorption [28] had shown a larger heat of adsorption on the Lewis sites.

Desorption from Brönsted site implies deprotonation and should fit a Langmuir isobar [29], represented by

$$N = N_{\text{sat}}\big(a\exp(b/T)/(1+a\exp(b/T))\big) \tag{1}$$

valid for a homogeneous surface. Generally the temperature at which $NH_4{}^+$ is completely desorbed is about 400 °C [29]. For H-zeolites, 175 °C in vacuum was considered at the limit beyond which only chemisorbed NH_3 subsists. Experimental and simulated Langmuir desorption isobars of pyridinium are shown in Fig. 9.

The desorption isobar from the Lewis sites obeys a Temkin law, or

$$\ln N = a + b/T, \tag{2}$$

where a and b are arbitrary constant. The Temkin isotherm applies to heterogeneous surfaces. In order to know the number of Lewis sites, a temperature limit must be chosen. Beyond this limit, it is assumed that chemisorbed species, only, subsist. For ammonia on acid zeolites, the temperature was set at 115 °C. In Table 2, the temperature has been set arbitrarily at 50 °C.

Fig. 10 shows Temkin desorption isobars of pyridine. The desorption energy (Table 4) is near 2 kcal/mol, except for B-50 where it is about 5 kcal/mol, suggesting that Lewis sites in B-50 are stronger.

The Brönsted site in the acidic form of a near-faujasite zeolite is not stronger than the sulfate-generated acid site on γ-Al_2O_3 since the complete deammoniation of the former occurs above 350 °C while the pyridinium cations on the sulfated alumina are removed near 400 °C, see Fig. 9. The desorption activation energy is near 6 kcal/mol (Table 4).

Table 4
Desorption activation energy, E_a, for Lewis and Brönsted sites (kcal/mol)

Sample	E_a, Lewis	E_a, Brönsted
B-50	5.1	–
B-100	1.8	5.9
B-140	2.4	5.8
B-180	2.2	–
B-240	3.2	–

The strength of Lewis sites is difficult to quantify. From the hyperfine splitting [30,31] of the aniline radical cation, weaker Lewis sites were found in a sulfated alumina than in sulfated zirconia. In transition aluminas rich in Al^V, the strength is less than that on nonframework alumina in HY steamed at 550 °C.

It would be interesting to examine the catalytic properties of sulfated aluminas in which Al^V is somewhat preserved. Yong et al. [32] had studied the model reaction 1-butene/*cis* and *trans* 2-butene and shown that the Lewis sites associated with Al^V enhance the *cis/trans* conversion in transition aluminas prepared by the sol–gel technique but with no hydrothermal aging. Since the energy barrier for the *2c/2t* conversion is the highest in the 1-butene isomerization reaction [33], it was concluded that the Lewis sites associated with Al^V were stronger.

The surface density in NH_3 chemisorbed with a heat of chemisorption larger than 120 kJ/mol (28.7 kcal/mol) on a γ-Al_2O_3 [29] was $\cong$ 0.7 μmol/m^2, while the activation energy for desorption was in the range quoted in Table 4. These figures are similar to those found in the present study.

5. Conclusions

Alumina gels obtained from $Al_2(SO_4)_3 \cdot 18H_2O$ and NH_4OH, aged hydrothermally between 50 and 240 °C for 18 h, and calcined at 600 °C for 4 h, offer the particu-

larity of displaying two types of acidity. Besides Lewis acid sites attributable to fourfold coordinated aluminum, strong Brönsted sites are present in the samples aged at temperatures lower than 180 °C. These sites would be made HSO_4^- anchored by two points to the surface, namely by sharing an oxygen with a coordinately unsaturated site and an oxygen with a tetrahedral aluminum.

As expected, the decomposition of 4-methylpentan-2-ol shows skeletal isomerization when Brönsted sites are present. The tuning of the type of acidity, by the temperature of the hydrothermal treatment, is an attractive feature of the suggested preparations.

Acknowledgments

The authors thank the Maya Crude Oil Research Program for financial support though Project D.01024. We also thank Professor A.L. Blumenfeld for the ^{27}Al MAS NMR spectra.

References

[1] K. Tanabe, Solid and Acids and Bases. Their Catalytic Properties, Academic Press, New York, 1970.
[2] K. Arata, Adv. Catal. 37 (1990) 165.
[3] K. Tanabe, H. Hattori, T. Yamaguchi, Crit. Rev. Surf. Chem. 1 (1995) 1.
[4] A. Corma, Chem. Rev. 95 (1995) 559.
[5] T. Yamaguchi, T. Jin, T. Ishida, K. Tanabe, Mater. Chem. Phys. 17 (1987) 3.
[6] K. Tanabe, Appl. Catal. A 113 (1994) 147.
[7] T.-S. Yang, T.-H. Chang, C.-T. Yeh, J. Mol. Catal. 115 (1997) 339.
[8] M.L. Ferreira, E.H. Rueda, J. Mol. Catal. 178 (2002) 147.
[9] D. Mishra, S. Anand, R.K. Pande, R.P. Das, Mater. Lett. 42 (2000) 38.
[10] M.L. Guzmán-Castillo, F. Hernández-Beltrán, A. Rodríguez-Hernández, A. Vazquez-Rodríguez, A.B. Mar-Mar, Proc. Ibero-American Catal. Conf. (2002) 1680.
[11] X. Bokhimi, J.A. Toledo-Antonio, M.L. Guzmán-Castillo, F. Hernández-Beltrán, J. Solid State Chem. 161 (2001) 319.
[12] M.C. Gastuche, A. Herbillon, Bull. Soc. Chim. Fr. (1962) 1404.
[13] F.R. Chen, J.G. Davis, J.J. Fripiat, J. Catal. 133 (1992) 263.
[14] D.J. Coster, J.J. Fripiat, Chem. Mater. 5 (1993) 1204.
[15] M.L. Guzmán-Castillo, X. Bokhimi, A. Toledo-Antonio, J. Salmones-Blásquez, F. Hernández-Beltrán, J. Phys. Chem. 105 (2001) 2099.
[16] T.R. Hughes, H.M. White, J. Phys. Chem. 71 (1967) 7.
[17] D.J. Rosemberg, J.A. Anderson, Catal. Lett. 83 (2002) 59.
[18] J. Sánchez-Valente, X. Bokhimi, F. Hernández-Beltrán, Langmuir 19 (9) (2003) 3583.
[19] M. Waqif, J. Bachelier, O. Saur, J.C. Lavalley, J. Mol. Catal. 72 (1992) 127.
[20] M. Bensitel, O. Saur, J.C. Lavalley, B.A. Morrow, Mater. Chem. Phys. 19 (1988) 147.
[21] J.R. Sohn, H.J. Kim, J. Mol. Catal. 52 (1989) 379.
[22] K. Nakamoto, Infrared Spectra of Inorganic and Coordination Compounds, 2nd ed., Wiley, New York, 1963.
[23] F. Babou, G. Coudurier, J. Vedrine, J. Catal. 152 (1995) 341.
[24] E. Zhao, Yu. Isaev, A. Sklyarov, J.J. Fripiat, Catal. Lett. 60 (1999) 173.
[25] P. Berteau, B. Delmon, J.-L. Dallons, A. Van Gysel, Appl. Catal. 70 (1991) 307.
[26] A. Auroux, P. Artizzu, I. Ferino, V. Solinas, G. Leofanti, M. Padovan, G. Messina, R. Mansani, J. Chem. Soc., Faraday Trans. 91 (1995) 3263.
[27] P. Sykes, in: A Guidebook to Mechanisms in Organic Chemistry, 5th ed., Longman, London, 1982, p. 240.
[28] A. Auroux, M. Muscas, D.J. Coster, J.J. Fripiat, Catal. Lett. 28 (1994) 79.
[29] V. Gruver, J.J. Fripiat, J. Phys. Chem. 98 (1994) 8549.
[30] F.R. Chen, J.J. Fripiat, J. Phys. Chem. 97 (1993) 5776.
[31] D.J. Coster, A. Bendada, F.R. Chen, J.J. Fripiat, J. Catal. 140 (1993) 497.
[32] H. Yong, D. Coster, F.R. Chen, J.G. Davis, J.J. Fripiat, in: New Frontiers in Catalysis, Proc. 10th Intl. Cong. Catal., Elsevier Science, Amsterdam, 1992, p. 1159.
[33] J.W. Hightower, W.K. Hall, J. Phys. Chem. 71 (1967) 1014.